# Three-Dimensional Finite Element Study on Li Diffusion Induced Stress in FIB-SEM Reconstructed LiCoO₂ Half Cell

Linmin Wu[1], Youhai Wen[2], Jing Zhang[1,*]

[1]Department of Mechanical Engineering, Indiana University-Purdue University Indianapolis, Indianapolis, IN 46202, USA

[2]National Energy Technology Laboratory,

Albany, OR 97321, USA

*Email: jz29@iupui.edu; Phone: 317-278-7186; Fax:317-274-9744

## Abstract

In this study, the diffusion induced stress of LiCoO₂ half cell with a realistic 3D microstructure has been studied using finite element method. The electrochemical properties under various C rates were studied. The discharged curves under various C rates were simulated. Results show that the potential drops significantly with the increase of C rates. The lithium ion concentration distribution under high discharging rates shows strong inhomogeneity. At high C rates, the small LiCoO₂ particles near the separator have higher lithium ion concentration because of the shorter lithium migration and diffusion paths. The diffusion induced stress inside LiCoO₂ particles was calculated coupled with lithium diffusion. The results show that the stress near the concave and convex regions is the highest. The neck regions of the connected particles will break first and form several isolated particles. For isolated particles, cracks are more likely to form on the surface rather than inside the particle. Failure may occur in large grains ahead of small grains.

**Keywords:** diffusion induced stress; FIB-SEM; LiCoO₂; finite element; microstructure

## 1. Introduction

Lithium ion rechargeable batteries (LIBs) have attracted many attentions since they are desirable energy storage devices. Many studies have been carried out to increase the performance and cycle life of LIB. Many concerns, such as thermal runaway [1-3], dendrites formation [4, 5], and side reactions [6, 7], have been investigated to understand the capacity loss and failure mechanisms. Among these concerns, one of the critical challenge of LIB is to prevent fracture and mechanical failure during lithium intercalation and deintercalation processes. Experiment observes that 20% $LiCoO_2$ particles fractured after 50 cycles under 0.2 C rate [8]. Thus, it is important to understand the diffusion induced stress in the battery materials.

Many works have been done to study the diffusion induced stress to improve the cycle life of LIBs [9-12]. Zhang et al. [11, 12] studied the diffusion induced stress in $LiMn_2O_4$ under galvanostatic and potentiodynamic conditions using ellipsoid shaped particle model. Cheng and Verbrugge [10] investigated the strain energy of a spherically-shaped electrode particle under a periodic voltage excitation source. They evaluated the crack nucleation using strain energy density method. Zhao et al. [9] studied the diffusion induced fracture of $Li_xCoO_2$ particles using fracture mechanics. However, many of these studies using single sphere particle model, and diffusion kinetics and electrochemical processes are simplified greatly.

There are some attempts to simulate the diffusion induced stress in porous intercalation electrode. Garcia et al. [13] studied the stress and electrochemical performance in a 2D model geometry with sphere particles distributed inside the porous electrode. Renganathan et al. [14] simulated the stress inside the porous electrode by taking advantage of the P2D model. Although the geometry and diffusion kinetics have been improved in these works, some important features can not be captured using homogeneous microstructures, such as the diffusion kinetics at high C

2

rates and the geometry effect on stress. Thus, a realistic microstructure based diffusion induced stress study is necessary.

To our best knowledge, realistic microstructure based stress studies in LIBs are limited. Lim et al. [15] calculated the stress in reconstructed graphite and $LiCoO_2$ single particles. The electrochemistry framework is simplified. Wu et al. [16] investigated the diffusion induced stress in $LiMn_2O_4$/C whole cell using realistic microstructure, but their model is in 2D. We recently simulated the diffusion induced stress in synchrotron X-ray tomography reconstructed Nickel-Manganese-Cobalt (NMC) based half cell [17]. Hence, a 3D realistic microstructure based diffusion induced stress model under the complex electrochemistry framework is warranted.

In this paper, the electrochemical performance and diffusion induced stress will be calculated in FIB-SEM reconstructed $LiCoO_2$ half cell. The paper will be organized as follows: In section 2, the details of imaging processing and reconstruction of $LiCoO_2$ half cell are given. In section 3, a set of mathematical formulations describing the electrochemistry and stress in LIBs are listed. In section 4, the potential response and lithium ion concentration under various C rates are studied. The geometry and particle size effect on stress are discussed. The stress distribution in the particles is also analyzed. Conclusions are given in section 5.

## 2. Image processing and domain generation

The cross-sectional images of LiCoO₂ cathode identified by FIB-SEM technique were reported in ref. [18]. The resolution of each gray-scale image is 35 nm × 35 nm × 62 nm. The image stack containing 200 images was imported into Avizo software for image processing and segmentation. As shown in the literature, the carbon phase is randomly distributed in the electrode and has a highly irregular shape. Due to the high computational cost and mesh generation difficulty, the carbon phase was neglected in this study. An Edge Preserving Smoothing Filter was applied followed by the greyscale threshold segmentation. The resulting reconstruction is a cuboid with a dimension of 20.02 μm × 18.13 μm × 12.04 μm.

In order to create the LiCoO₂ half cell, the separator with 4 μm thickness were added to the cathode domain (Fig. 1). The pore space in the cathode domain was filled with electrolyte. The porous structure in the separator was neglected. The three domains were meshed and imported into Comsol Multiphysics for further simulation.
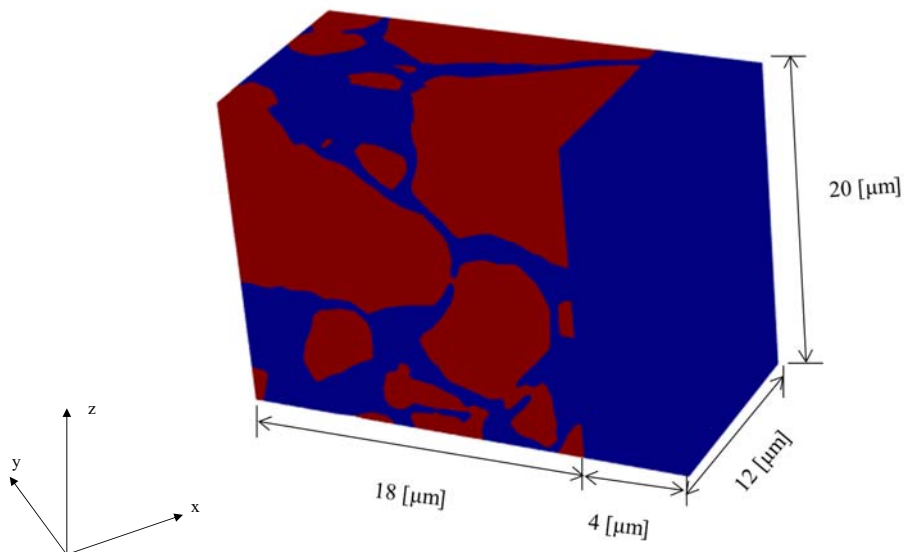
Fig. 1: Illustration of LiCoO$_2$ half cellRed color represents LiCoO$_2$, and blue color represents electrolyte.

### 3. Model description

The mathematical model consists of electrochemistry sub-model and mechanics sub-model. The electrochemistry model describes the species and charge transports in LiCoO$_2$ half cell. The mechanics model computes the mechanical stress and diffusion induced stress in active particles.

3.1 Electrochemistry

The electrochemistry model describing battery kinetics, mass and charge transports is based on the work of Doyle et al. [19] and Fuller et al. [20]. In order to distinguish different domains, subscript of $i = 1$, and 2 denotes the active cathode particles and the electrolyte.

*Active cathode particles* — The charge balance in the active cathode particles follows the Ohm's law:

$$\nabla \cdot (-k_1 \nabla \phi_1) = \nabla \cdot J_1 = 0 \tag{1}$$

where $k_1$ is the electrical conductivity of the active cathode particles; $\phi_1$ is the electrical potential and $J_1$ is the current density in LiCoO$_2$ particles.

It is shown that the ideal solution thermodynamics assumption was applied in describing the transport of lithium ions and diffusion induced stress, and is widely used in battery modeling [12-14, 21-23]. Hence, the transport of Lithium ions in active particles is described by the modified Fick's law [12, 24], which includes the effect of stress on diffusion:

$$\frac{\partial c_1}{\partial t} + \nabla \cdot \left( -D_1 \nabla c_1 + \frac{D_1 \Omega c_1}{RT} \nabla \sigma_h \right) = 0 \qquad (2)$$

where $c_1$ is the lithium ion concentration in solid particles; $D_1$ is the diffusivity of lithium ions in LiCoO$_2$; R is the universal gas constant; T is the temperature, which is set 300 K in this study; $\Omega$ is the partial molar volume of active particles; $\sigma_h = (\sigma_{11} + \sigma_{22} + \sigma_{33})/3$ is the hydrostatic stress ($\sigma_{ij}$ is the stress component in the stress tensor).

*Electrolyte* — The charge transport equation of the electrolyte phase couples the concentration of lithium ions and the electrical potential, and has the following form:

$$\nabla \cdot \left( -k_2 \nabla \phi_2 + \frac{2k_2 RT}{Fc_2}\left(1 + \frac{\partial lnf_2}{\partial lnc_2}\right)(1 - t_+)\nabla c_2 \right) = \nabla \cdot J_2 = 0 \qquad (3)$$

where $k_2$ is the electrical conductivity of the electrolyte, $\phi_2$ is the electrical potential; F is the Faraday constant; $c_2$ is the lithium ion concentration in the electrolyte; $t_+$ is the transference number of positive ions, which is set 0.363 in this study; $f_2$ is the mean molar activity coefficient of the electrolyte.

The mass transport of lithium ions in the electrolyte is expressed as:

$$\frac{\partial c_2}{\partial t} + \nabla \cdot \left[ -D_2 \left(1 - \frac{dlnc_0}{dlnc_2}\right)\nabla c_2 + \frac{J_2 t_+}{F}\right] = 0 \qquad (4)$$

where $D_2$ is the reference lithium ion diffusivity in the electrolyte; $dlnc_0/dlnc_2$ is the concentrated solution correction to salt diffusivity; $J_2$ is the current density in the electrolyte. Assume the solvent concentration is not a function of the electrolyte [25], the term $dlnc_0/dlnc_3$ will be neglected. Since $t_+$ is a constant in this study, $\nabla \cdot (J_2 t_+/F)$ becomes zero.

*Interface conditions* — The chemical kinetics at the particle-electrolyte interface is described by the Butler-Volmer relationship:

$$N = \frac{i_n}{F} = \frac{i_0}{F} \times \left\{ \exp\left[\frac{(1-\alpha)F\eta}{RT}\right] - \exp\left[\frac{-\alpha F\eta}{RT}\right] \right\} \tag{5}$$

where N is the flux of lithium ions; $i_0$ is the exchange current density; $\alpha$ is the cathodic charge transfer coefficient, which is 0.5 in this study; $\eta$ is the overpotential at the particle-electrolyte interface.

The exchanged current density is defined as follows:

$$i_0 = Fk_0(c_2)^{1-\alpha}(c_\theta)^{1-\alpha}\left(c_{1,surf}\right)^\alpha \tag{6}$$

where $k_0$ is the reaction rate; $c_{1,surf}$ is the concentration of lithium ions on the surface of solid electrode; $c_\theta$ is the concentration of available vacant sites on the surface of solid particles.

The overpotential is given by:

$$\eta = \phi_1 - \phi_2 - U \tag{7}$$

where U is the open circuit potential at the interface.

3.2 Mechanics

The mechanics model computes the stress and particle deformation inside the LiCoO$_2$ half cell. The total strain $\varepsilon_{ij}$ of the active particles contains the mechanical strain $\varepsilon_{ij}^{me}$ and the diffusion induced strain $\varepsilon_{ij}^{dis}$. The diffusion induced strain is formulated by the thermal analogy [10, 14]. The constitutive equation describing the stress and strain is given by:

$$\varepsilon_{ij} = \varepsilon_{ij}^{me} + \varepsilon_{ij}^{dis} = \frac{1}{E}\left[(1+\upsilon)\sigma_{ij} - \upsilon\sigma_{kk}\delta_{ij}\right] + \frac{\hat{c}\Omega}{3}\delta_{ij} \tag{8}$$

where E is Young's modulus; $\upsilon$ is Poisson's ratio; $\sigma_{ij}$ is stress tensor; $\hat{c}$ is the concentration difference of lithium ions from the original value; $\Omega$ is the partial molar volume.

The stress components obey mechanical equilibrium:

$$\sigma_{ij,j} = 0 \tag{9}$$

Following ref. [13], the electrolyte was modeled as a compliance gel, which has a much lower Young's modulus than LiCoO$_2$ [26].

### 3.3 Boundary conditions and material properties

The electrochemistry boundary conditions are illustrated in Fig. 2 (a). At the left side of the current collector, a constant current density was applied. Different C rates were applied to simulate the discharge of LiCoO$_2$ half cell. C rates were calculated based on the volume of LiCoO$_2$ particles, specific capacity of LiCoO$_2$ (0.137 Ah/g) and the cross section area of the half cell. The corresponding 1C rate is 8.6216 A/m$^2$. At the right side of the electrolyte, the electric potential was set 0 V. For all other outer surfaces, no flux boundary conditions were applied.

The boundary conditions for mechanics model are shown in Fig. 2 (b). Since the cathode domain in this study is a portion of entire cathode, the symmetry boundary conditions were set at the upper, lower and left sides. At the right side of the electrolyte, fixed boundary condition was applied.
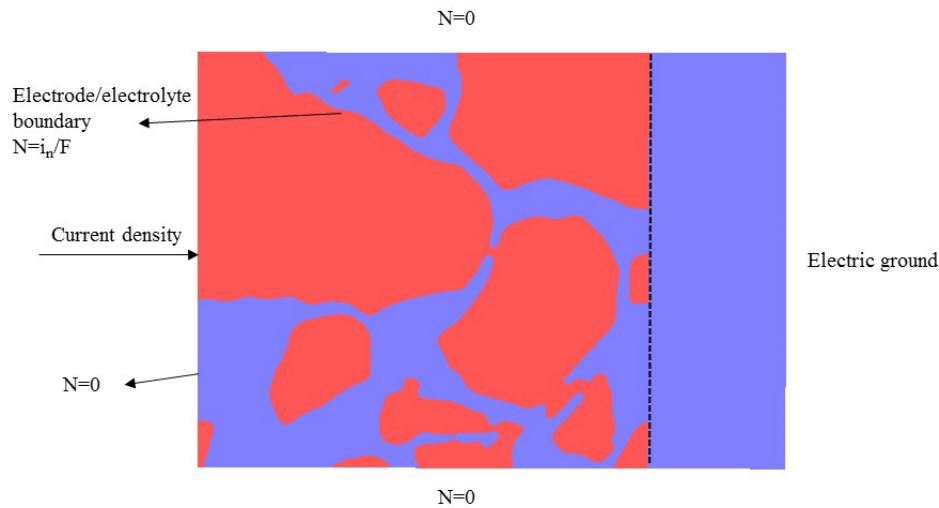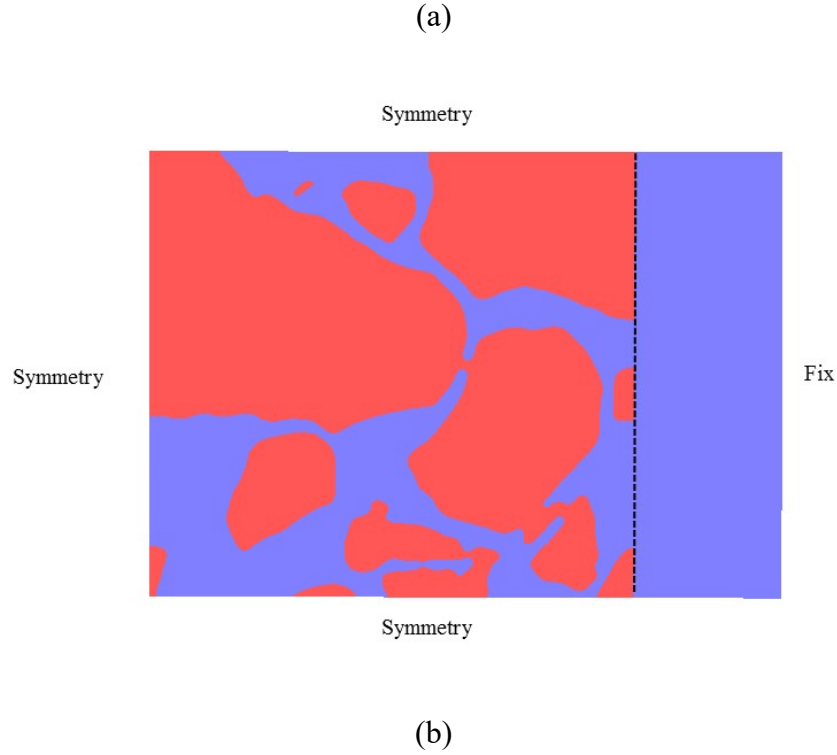
Fig. 2: Boundary conditions in LiCoO$_2$ half cell. (a) electrochemistry model; (b) mechanics model. Red color represents LiCoO$_2$, and blue color represents electrolyte.

The material properties used in the model are listed in Table 1. For electrical conductivity, lithium ion diffusivity and other related parameters in the electrolyte were those at 25 °C as provided in ref. [27]. The open circuit potential of LiCoO$_2$ and reaction rate constant at the cathode-electrolyte interface was chosen from ref. [28].

Table 1 Material properties used in the model

|  | LiCoO$_2$ | Current collector | electrolyte |
|---|---|---|---|
| Initial concentration (mol/m$^3$) | 25777 | / | 1000 |
| Maximum concentration (mol/m$^3$) | 51555 [29] | / | / |
| Electrical conductivity (S/m) | 10 [28] | $3.5 \times 10^7$ [16] | See ref. [27] |

| Diffusivity ($m^2$/s) | $1\times10^{-13}$ [29] | / | See ref. [27] |
|---|---|---|---|
| Young's modulus (GPa) | 70 [14] | / | 0.001 [13] |
| Poisson's ratio | 0.3 [14] | / | 0.25 [13] |
| Partial molar volume ($m^3$/mol) | $-1.947\times10^{-6}$ [30] | / | / |

## 4. Results and discussion

The mathematical model described in section 3 was implemented in Comsol Multiphysics PDE module. The simulation time step was set 0.001 s. The $LiCoO_2$ half cell discharged under various C rates was simulated. In this study, the $LiCoO_2$ half cell was discharged during the state of charge (SOC) from 0.5 to 1. The state of charge was defined as the ratio of the maximum local lithium ion concentration to the stoichiometric lithium ion concentration in $LiCoO_2$ particles. The initial SOC for discharge was set 0.5, because experiment observes that lithium ions can't intercalate into $Li_xCoO_2$ particles if x<0.5 [31].

### 4.1 Electrochemical response

The simulated discharge curve of $LiCoO_2$ half cell was shown in Fig. 3. The half cell discharged at 0.5 C rate has the best electrochemical performance. At 5 C, the potential drops significantly compared with the 0.5 C and 1C case. At the end of discharge, the potential of the cell discharged at 5 C is 0.24 V lower than the 0.5 C. The large internal resistance at high current density causes this phenomenon.
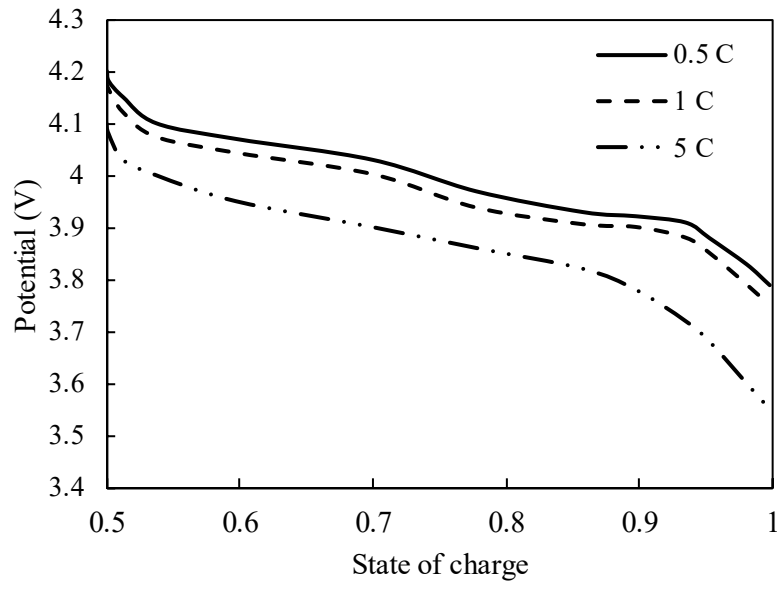
Fig. 3: Simulated discharge curves of LiCoO$_2$ half cell under 0.5 C, 1C and 5 C rates.

The lithium ion concentration profiles at SOC=1 under various C rates were shown in
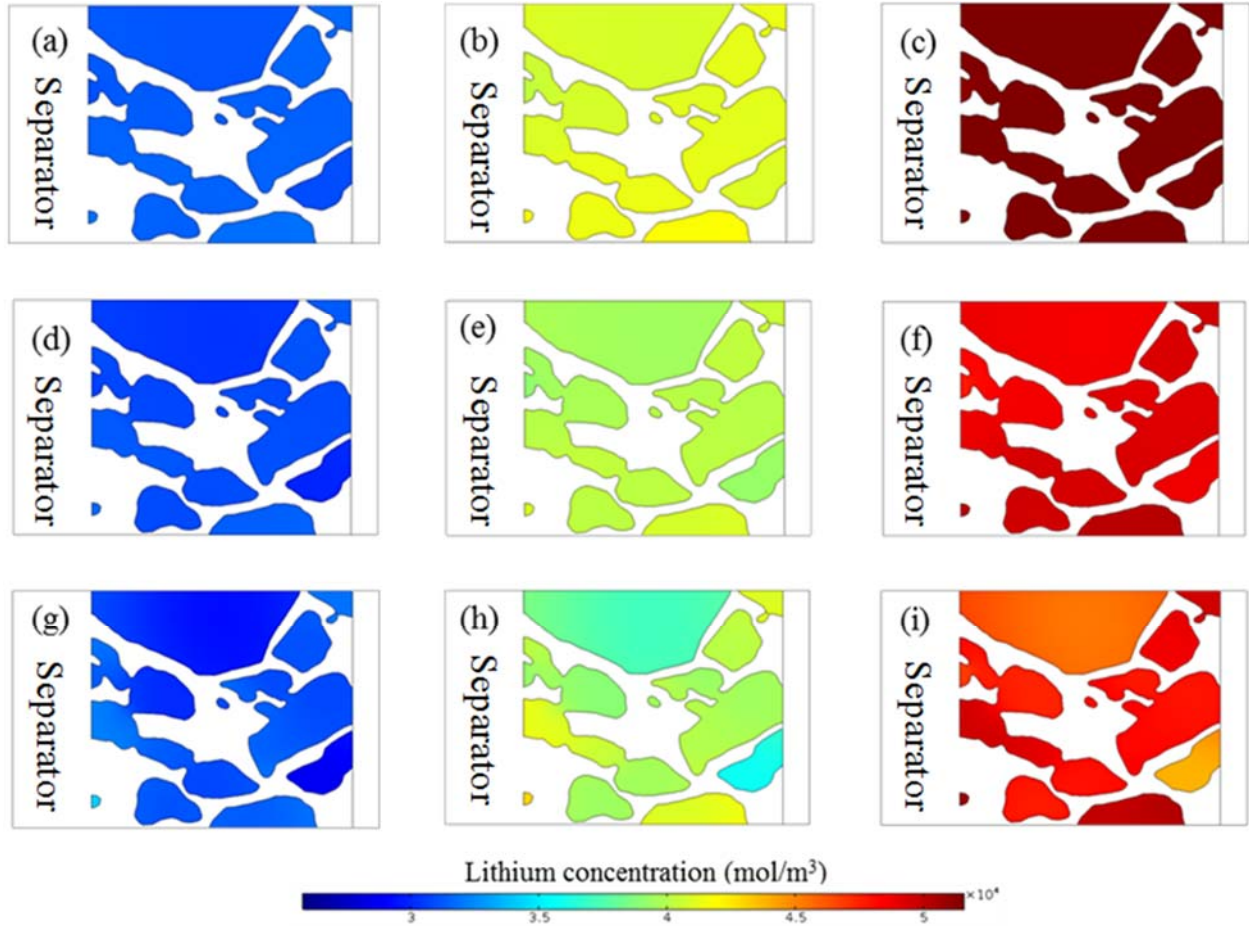


Lithium concentration (mol/m³)

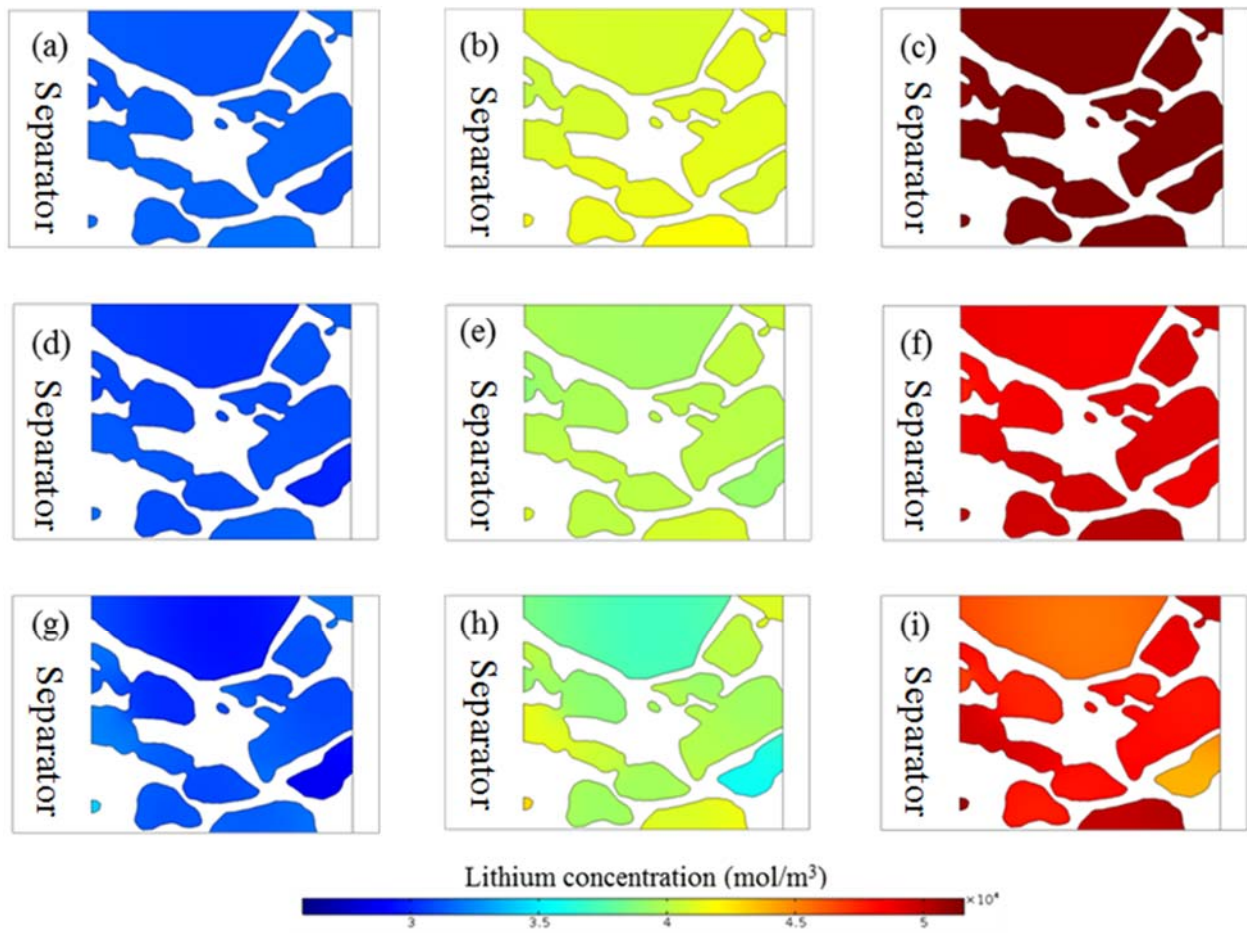Fig. 4. At 0.5 C, the lithium ion concentration distribution at the end of discharge is homogeneous (see

Fig. 4 (a), (b) and (c)). With the increase of the current density, the spatial lithium ion
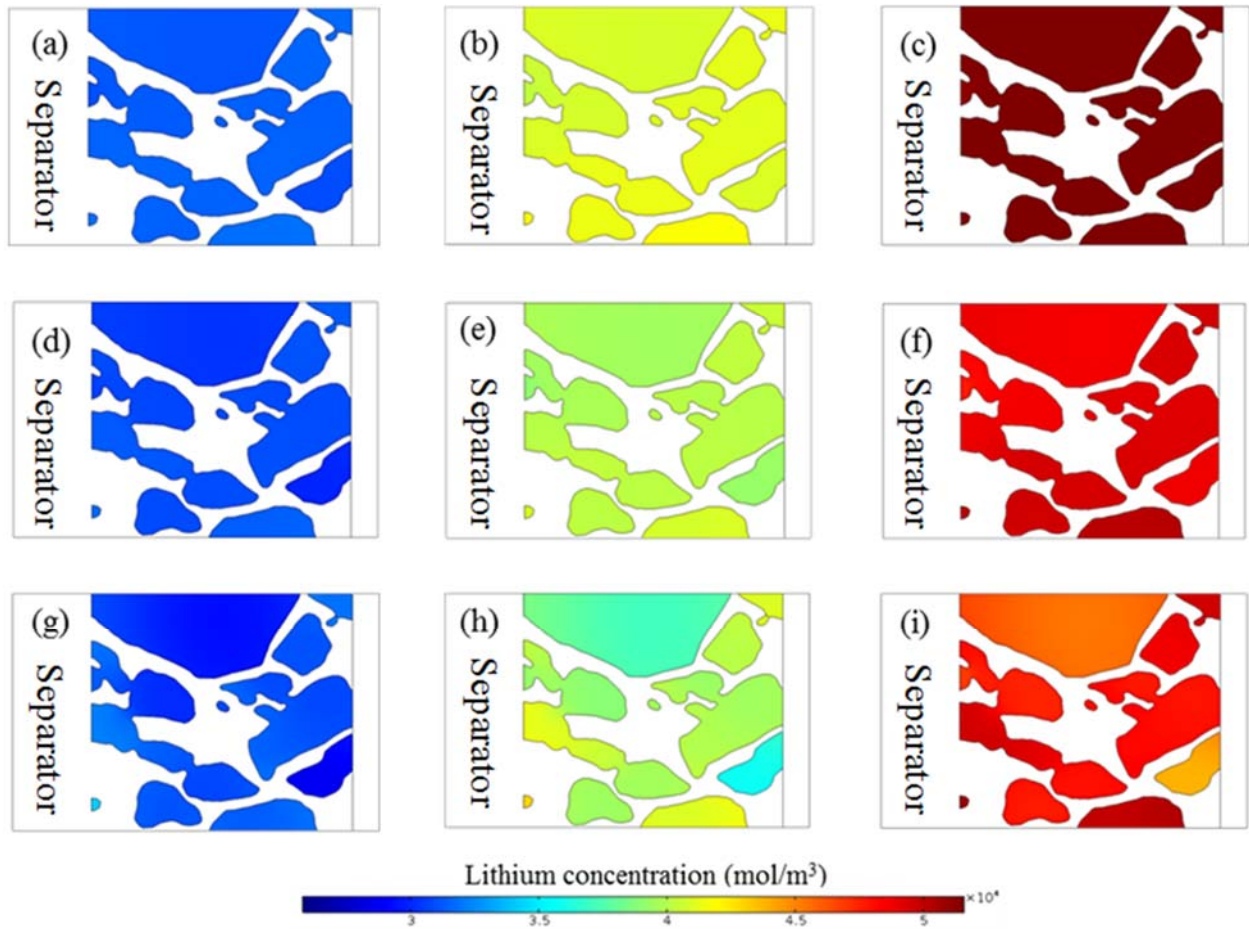
concentration becomes more inhomogeneous (see



Fig. 4 (d), (e), (f), (g), (h) and (i)). This is due to the position and size of the LiCoO$_2$ particles.

Here are some observations: (1) The smaller the LiCoO$_2$ particles, the easier for lithium ions

intercalate into the active material. This causes higher lithium ion concentration in these particles.

It can be explained by the shorter diffusion distance from the particle surface to the middle. (2)

The more the LiCoO$_2$ particles away from the separator (separator is the lithium source during the

discharge process), the less likely for lithium ions to diffuse into the particles. It leads lower lithium

ion concentration in the particles. The reason can be contributed to the longer migration paths of

lithium ions from the separator. Hence, combined (1) and (3), the smaller LiCoO$_2$ particles near

the separator have higher lithium ion concentration, and larger particles near the current collector has lower lithium ion concentration. In realistic geometry model, the inhomogeneous size and distribution of active materials causes the inhomogeneity of the electrochemical properties. This is what traditional 1D model failed to predict.
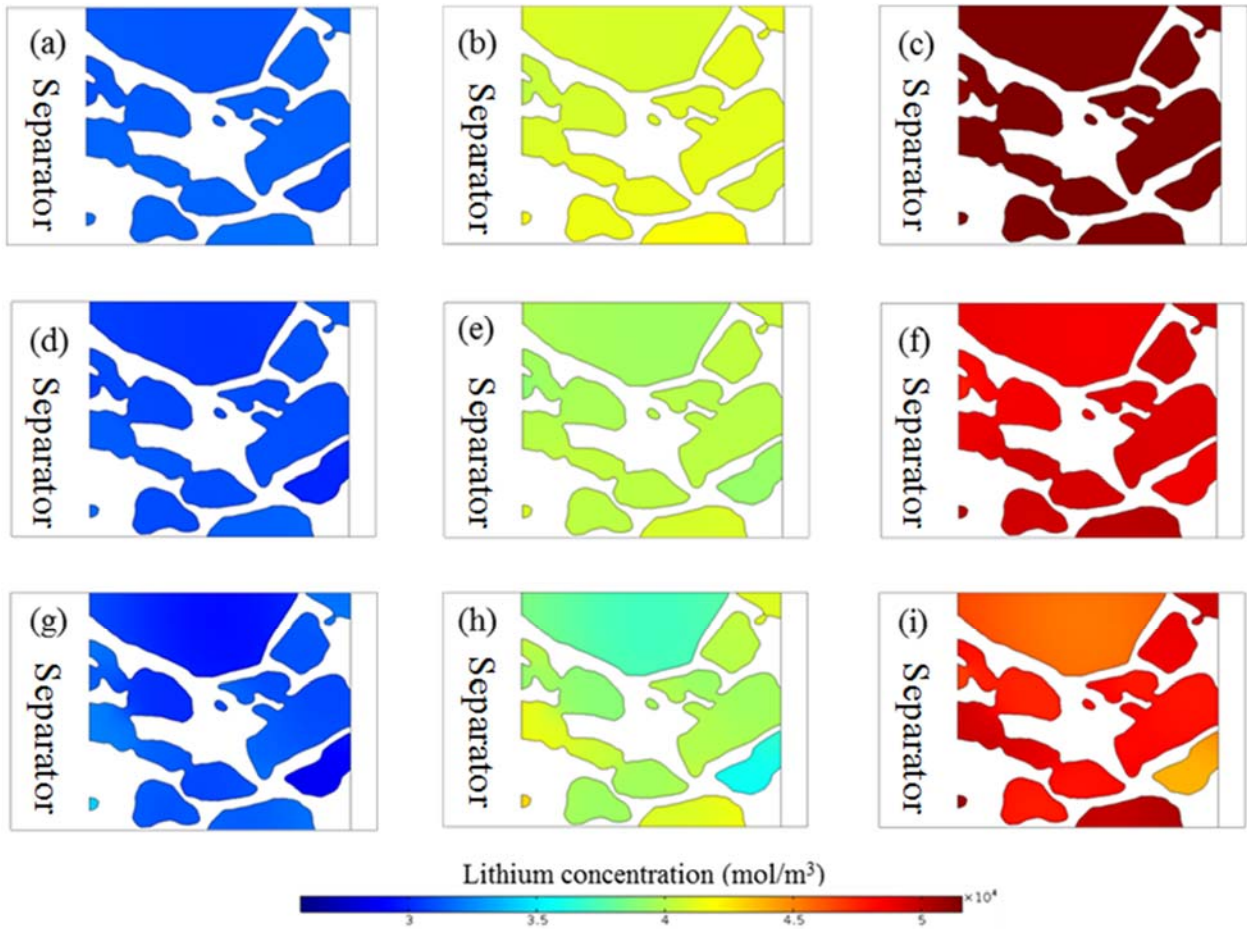


Fig. 4: Lithium ion concentration in LiCoO$_2$ particles under various C rates. The figures are taken from the cross section of the half cell which positioned at z=10 μm.

(a) SOC=0.6 under 0.5 C. (b) SOC=0.8 under 0.5 C (c) SOC=1 under 0.5 C

(d) SOC=0.6 under 1 C (e) SOC=0.8 under 1 C (f) SOC=1 under 1 C

(g) SOC=0.6 under 5 C (h) SOC=0.8 under 0.5 C (i) SOC=1 under 5 C

4.2 Stress response

The failure of the brittle materials is often related to the tensile stress [21]. In order to capture the failure inside the LiCoO$_2$ cathode, the 1st principal stresses insede the cathode were calculated. The maximum 1st principal stresses in LiCoO$_2$ particles under 0.5 C, 1 C and 5 C rates are shown in Fig. 5. Under galvanostatic discharge conditions, the stress levels increase monotonically. With the increase of the discharging current density, the maximum tensile stresses increase. The maximum stress at 5 C is 153 MPa, which is about 50% larger than the 1 C case and 120% larger than the 0.5 C case. Since the yield strengh of LiCoO$_2$ is around 100 MPa [14], it is predicted that the LiCoO2 cathode will experience fracture under 5 C discharging rate.
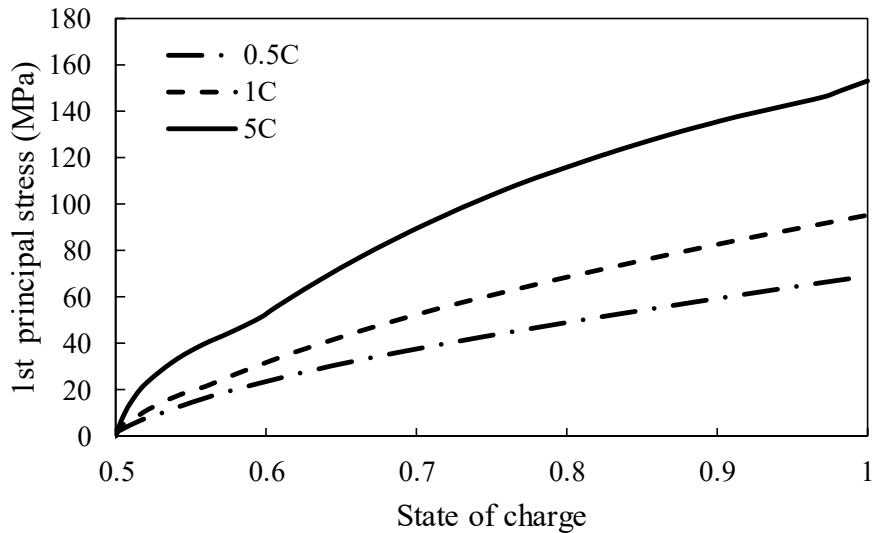


Fig. 5: Time history of maximum 1st principal stress in LiCoO$_2$ particles under 0.5 C, 1 C and 5 C rates.

To better understand the failure mechanisms in the LiCoO$_2$ half cell, the stress distribution inside the particles was investigated. In Fig. 6, the 1st principal stress distribution inside the LiCoO$_2$

particles at SOC=1 under 5 C rate is shown. Unlike the uniform stress distribution in 1D model [32] and single particle model [12], the stress distribution shows strong geometry effect. There are some features for stress distribution: (1) In the concave and convex regions, the 1st principal stresses are much higher than other areas (case A). (2) For isolated $LiCoO_2$ particles, the stresses in large grains are higher than small grains if there is no stress concentraion near the connecting regions (case B). (3) If the $LiCoO_2$ particles are isolated, the stresses on the surface of the $LiCoO_2$ particles are higher than the stresse on the surface (case C), which is in agreement with previous simulation observations [16]. Since the stresses near the concave and covex regions are the highest, the cracks may be initiated in these regions. Once the cracks propogate, the neck regions of the connected particles will break and form several isolated particles. For isolated particles, cracks are more likely to form on the surface rather than inside the particles. Failure may occur in large grains ahead of small grains.
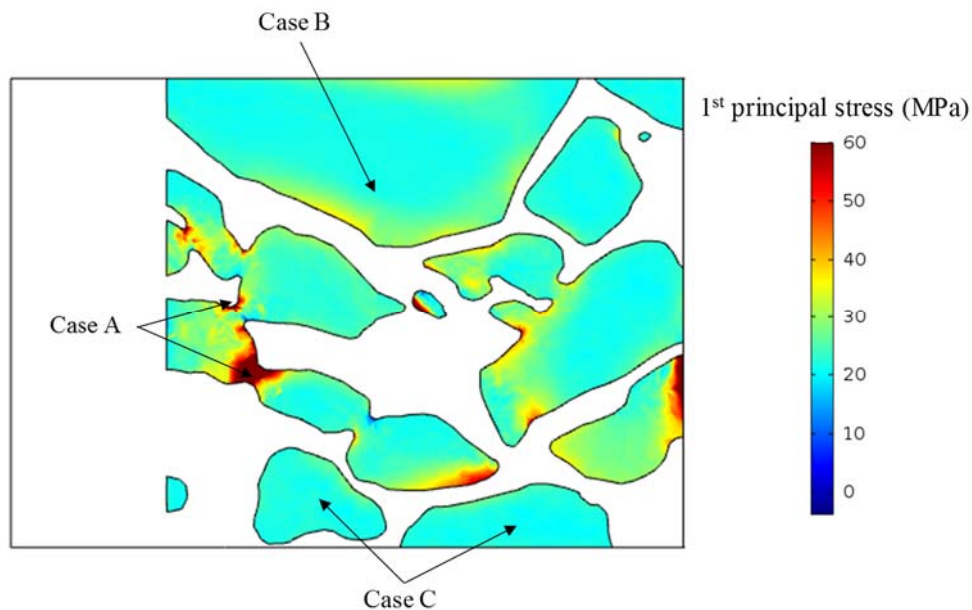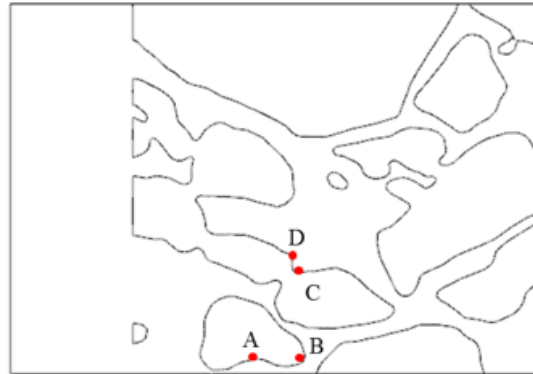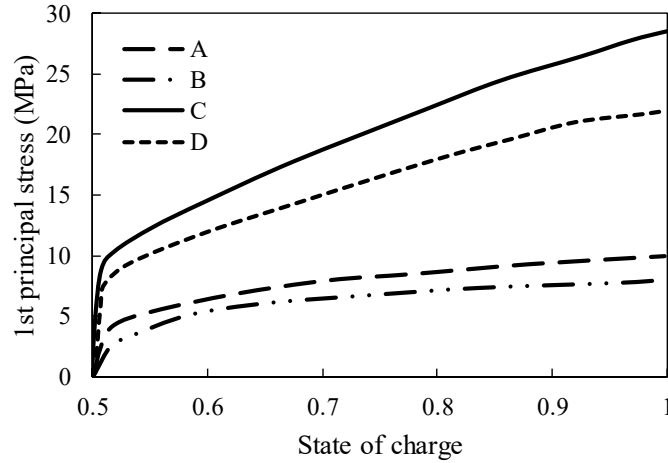


Fig. 6: 1st principal stress distribution in reconstructed $LiCoO_2$ particles at SOC=1 under 5 C rate. The figures are taken from the cross section of the half cell which positioned at z=10 μm.

To study the geometry effect more quantitatively, the stress distribution near the convex and concave regions was investigated. In the study, four points were selected to represent the concave and convex regions, as shown in Fig. 7 (a). A and C represent the concave regions, while B and D represent the convex regions. The 1$^{st}$ principal stress time history of four points under 1 C rate was shown in Fig. 7 (b). The stresses of all of the four points shows the similar pattern as Fig. 5. The stress levels increase with the discharging time. The 1$^{st}$ principal stresses of two concave points A and C are higher than the corresponding convex points B and D. The maximum principal stress of point A is 28.9 MPa, which is about 32% higher than the stress of point B. The maximum stress of point C is 25% larger than its corrospoonding convex point D. Hence, the maximum tensile stress is more likely to occur at concave regions rather than convex regions.



(a)

(b)

Fig. 7: (a) The positions of four selected points A, B, C and D. (b) The 1$^{st}$ principal stress time history of four selected points A, B, C and D under 1 C rate.

To study the stress distribution inside the LiCoO$_2$ particles, two lines were selected in an isolated single particle. L1 is the horizontal line inside the particle, while L2 is the verticle line. The positions of two lines are shown in Fig. 8 (a). The 1$^{st}$ principal stress distributions along L1 and L2 are shown in Fig. 8 (b). The stress distribution along L1 and L2 shows similar features. On particle surfaces, the stress has the largest value along both lines. The minimum magnitude is reached in the middle of L1 and L2. In order to explain this phenomenon, the lithium concentration gradient along these two lines was investigated. Here, the lithium concentration gradient is defined as the difference of the local lithium concentration and the mean lithium concentration. As shown in Fig. 8 (b), the lithium ion concentration gradient has the smallest value in the middle of the particle. Hence, the diffusion induced strain becomes the lowest in the middle of L1 and L2 and the highesr at two ends of L1 and L2 according to the equation (8). Thus, cracks may initiated on the surfaces of the particle.
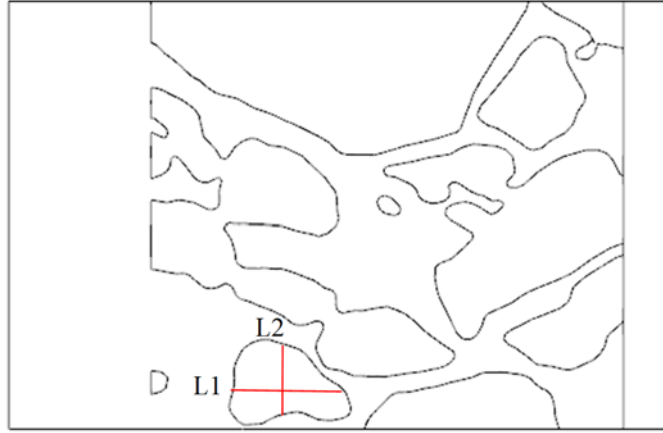
(a)
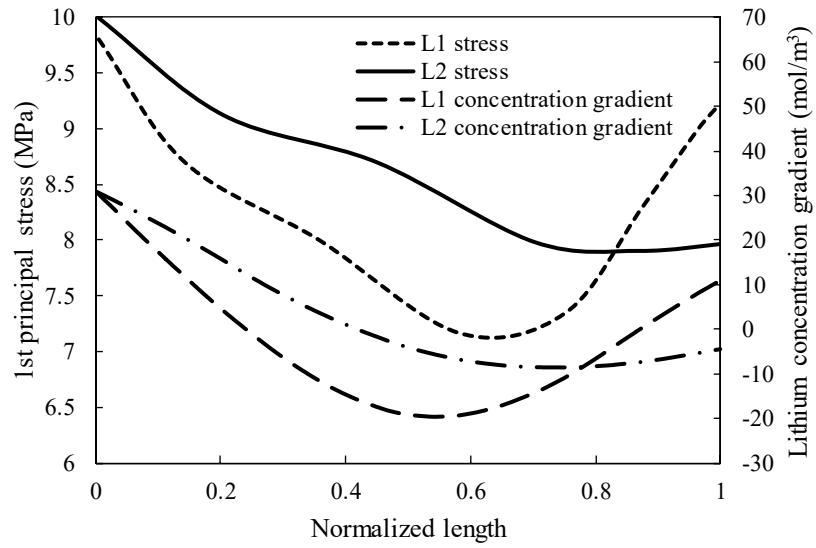


(b)

Fig. 8: (a) The positions of two selected lines L1 and L2. (b) The 1st principal stress and lithium concentration gradient of L1 and L2 under 1 C rate.

### 5. Conclusions

In this paper, the electrochemical properties and diffusion induced stresses in LiCoO$_2$ with realistic 3D microstructures have been investigated using finite element method. The conclusions are summarized as follows:

(1) The discharged curves under various C rates were simulated. The potential drops significantly with the increase of C rates.

(2) The lithium ion concentration distribution under high discharging rates shows strong inhomogeneity. At high C rates, the small LiCoO$_2$ particles near the separator have higher lithium ion concentration because of the shorter lithium migration and diffusion paths.

(3) The maximum 1$^{st}$ principal stress under different C rates increases at the initial stage and then decreases. The maximum stress at 5 C is 153 MPa, which is about 50% larger than the 1 C case and 120% larger than the 0.5 C case.

(4) The maximum stress is more likely to occur at concave regions rather than convex regions. The study shows the maximum tensile stresses in the concave region can be 32% larger than the convex region.

(5) For isolated LiCoO$_2$ particles, the fracture is more likely to occur on the surface rather than inside the particles. The high surface stress can be contributed to the higher lithium concentration gradient on the surface.

(6) Failures are more likely to occur in large grains.

# Acknowledgement

# References

[1]     A. W. Golubkov, D. Fuchs, J. Wagner, H. Wiltsche, C. Stangl, G. Fauler, *et al.*, "Thermal-runaway experiments on consumer Li-ion batteries with metal-oxide and olivin-type cathodes," *RSC Advances,* vol. 4, pp. 3633-3642, 2014.

[2]     D. P. Finegan, M. Scheel, J. B. Robinson, B. Tjaden, I. Hunt, T. J. Mason, *et al.*, "In-operando high-speed tomography of lithium-ion batteries during thermal runaway," *Nat Commun,* vol. 6, 04/28/online 2015.

[3]     Q. Wang, P. Ping, X. Zhao, G. Chu, J. Sun, and C. Chen, "Thermal runaway caused fire and explosion of lithium ion battery," *Journal of Power Sources,* vol. 208, pp. 210-224, 2012.

[4]     D. R. Ely and R. E. García, "Heterogeneous Nucleation and Growth of Lithium Electrodeposits on Negative Electrodes," *Journal of The Electrochemical Society,* vol. 160, pp. A662-A668, 2013.

[5]     K. J. Harry, D. T. Hallinan, D. Y. Parkinson, A. A. MacDowell, and N. P. Balsara, "Detection of subsurface structures underneath dendrites formed on cycled lithium metal electrodes," *Nat Mater,* vol. 13, pp. 69-73, 2014.

[6]     J. Xu, R. D. Deshpande, J. Pan, Y.-T. Cheng, and V. S. Battaglia, "Electrode Side Reactions, Capacity Loss and Mechanical Degradation in Lithium-Ion Batteries," *Journal of The Electrochemical Society,* vol. 162, pp. A2026-A2035, 2015.

[7]     C. K. Chan, R. Ruffo, S. S. Hong, R. A. Huggins, and Y. Cui, "Structural and electrochemical study of the reaction of lithium with silicon nanowires," *Journal of Power Sources,* vol. 189, pp. 34-39, 2009.

[8]     H. Wang, Y. I. Jang, B. Huang, D. R. Sadoway, and Y. M. Chiang, "TEM Study of Electrochemical Cycling-Induced Damage and Disorder in LiCoO2 Cathodes for Rechargeable Lithium Batteries," *Journal of The Electrochemical Society,* vol. 146, pp. 473-480, 1999.

[9]     K. Zhao, M. Pharr, J. J. Vlassak, and Z. Suo, "Fracture of electrodes in lithium-ion batteries caused by fast charging," *Journal of Applied Physics,* vol. 108, p. 073517, 2010.

[10]    Y.-T. Cheng and M. W. Verbrugge, "Evolution of stress within a spherical insertion electrode particle under potentiostatic and galvanostatic operation," *Journal of Power Sources,* vol. 190, pp. 453-460, 2009.

[11]    X. Zhang, A. M. Sastry, and W. Shyy, "Intercalation-Induced Stress and Heat Generation within Single Lithium-Ion Battery Cathode Particles," *Journal of The Electrochemical Society,* vol. 155, pp. A542-A552, 2008.

[12]    X. Zhang, W. Shyy, and A. Marie Sastry, "Numerical Simulation of Intercalation-Induced Stress in Li-Ion Battery Electrode Particles," *Journal of The Electrochemical Society,* vol. 154, pp. A910-A916, 2007.

[13]    R. E. García, Y.-M. Chiang, W. Craig Carter, P. Limthongkul, and C. M. Bishop, "Microstructural Modeling and Design of Rechargeable Lithium-Ion Batteries," *Journal of The Electrochemical Society,* vol. 152, pp. A255-A263, January 1, 2005 2005.

[14]    S. Renganathan, G. Sikha, S. Santhanagopalan, and R. E. White, "Theoretical Analysis of Stresses in a Lithium Ion Cell," *Journal of The Electrochemical Society,* vol. 157, pp. A155-A163, 2010.

[15]    C. Lim, B. Yan, L. Yin, and L. Zhu, "Simulation of Diffusion-Induced Stress Using Reconstructed Electrodes Particle Structures Generated by Micro/Nano-CT," *Electrochimica Acta,* vol. 75, pp. 279-287, 2012.

[16]    W. Wu, X. Xiao, M. Wang, and X. Huang, "A Microstructural Resolved Model for the Stress Analysis of Lithium-Ion Batteries," *Journal of The Electrochemical Society,* vol. 161, pp. A803-A813, 2014.

[17]    L. Wu, X. Xiao, Y. Wen, and J. Zhang, "Three-dimensional finite element study on stress generation in synchrotron X-ray tomography reconstructed nickel-manganese-cobalt based half cell," *Journal of Power Sources,* vol. 336, pp. 8-18, 12/30/ 2016.

[18]    T. Hutzenlaub, S. Thiele, R. Zengerle, and C. Ziegler, "Three-Dimensional Reconstruction of a $LiCoO_2$ Li-Ion Battery Cathode," *Electrochemical and Solid-State Letters,* vol. 15, pp. A33-A36, 2011.

[19]    M. Doyle, T. F. Fuller, and J. Newman, "Modeling of Galvanostatic Charge and Discharge of the Lithium/Polymer/Insertion Cell," *Journal of The Electrochemical Society,* vol. 140, pp. 1526-1533, 1993.

[20]    T. F. Fuller, M. Doyle, and J. Newman, "Simulation and Optimization of the Dual Lithium Ion Insertion Cell," *Journal of The Electrochemical Society,* vol. 141, pp. 1-10, 1994.

[21]    J. Park, W. Lu, and A. M. Sastry, "Numerical Simulation of Stress Evolution in Lithium Manganese Dioxide Particles due to Coupled Phase Transition and Intercalation," *Journal of The Electrochemical Society,* vol. 158, pp. A201-A206, 2011.

[22]    H. Mendoza, S. A. Roberts, V. E. Brunini, and A. M. Grillet, "Mechanical and Electrochemical Response of a LiCoO2 Cathode using Reconstructed Microstructures," *Electrochimica Acta,* vol. 190, pp. 1-15, 2/1/ 2016.

[23]    L. Wu, Y. Zhang, Y.-G. Jung, and J. Zhang, "Three-dimensional phase field based finite element study on Li intercalation-induced stress in polycrystalline LiCoO2," *Journal of Power Sources,* vol. 299, pp. 57-65, 12/20/ 2015.

[24]    F. Yang, "Interaction between diffusion and chemical stresses," *Materials Science and Engineering: A,* vol. 409, pp. 153-159, 2005.

[25]    J. Newman, "Electrochemical Systems, 3rd Ed.," *Wiley Inter-science, United States,* 2004.

[26]    L. Wu and J. Zhang, "Ab initio study of anisotropic mechanical properties of LiCoO2 during lithium intercalation and deintercalation process," *Journal of Applied Physics,* vol. 118, p. 225101, 2015.

[27]    W. Wu, X. Xiao, and X. Huang, "The effect of battery design parameters on heat generation and utilization in a Li-ion cell," *Electrochimica Acta,* vol. 83, pp. 227-240, 2012.

[28]    K. Kumaresan, G. Sikha, and R. E. White, "Thermal Model for a Li-Ion Cell," *Journal of The Electrochemical Society,* vol. 155, pp. A164-A171, 2008.

[29]    P. Ramadass, B. Haran, R. White, and B. N. Popov, "Mathematical modeling of the capacity fade of Li-ion cells," *Journal of Power Sources,* vol. 123, pp. 230-240, 2003.

[30]    T. Motohashi, Y. Katsumata, T. Ono, R. Kanno, M. Karppinen, and H. Yamauchi, "Synthesis and Properties of $CoO_2$, the x = 0 End Member of the $Li_xCoO_2$ and $Na_xCoO_2$ Systems," *Chemistry of Materials,* vol. 19, pp. 5063-5066, 2007.

[31]    Q. Zhang, Q. Guo, and R. E. White, "Semi-empirical modeling of charge and discharge profiles for a LiCoO2 electrode," *Journal of Power Sources,* vol. 165, pp. 427-435, 2007.

[32]    W. Wu, X. Xiao, X. Huang, and S. Yan, "A multiphysics model for the in situ stress analysis of the separator in a lithium-ion battery cell," *Computational Materials Science,* vol. 83, pp. 127-136, 2014.